

---

# Density Functional Study of $\text{FeO}_2$ , $\text{FeO}_2^+$ , and $\text{FeO}_2^-$

---

ALFONSO T. GARCÍA-SOSA, MIGUEL CASTRO

*Departamento de Física y Química Teórica, Facultad de Química, Universidad Nacional Autónoma de México, Del. Coyoacán, 04510, México D.F., México*

*Received 26 January 2000; revised 16 May 2000; accepted 16 May 2000*

---

**ABSTRACT:** The lowest energy structures of  $\text{FeO}_2$  were determined by means of density functional theory techniques as implemented in the program DGauss 3.0.1. The calculations performed were of the all-electron type using two levels of theory, namely the local spin density approximation with the use of the Vosko–Wilk–Nusair (VWN) functional and the generalized gradient approximation (GGA) in the form of the Becke (1988) exchange and Perdew (1986) correlation functionals. Results were visualized by means of the program UniChem. Bond distances and angles as well as total energies were calculated for several states of the moieties:  $\text{Fe}(\text{O})_2$ ,  $C_{2v}$ ;  $\text{Fe}(\text{O})_2$ ,  $D_{\infty h}$ ;  $\text{Fe}(\eta^2\text{-O}_2)$ ,  $C_{2v}$ ;  $\text{Fe}(\eta^1\text{-O}_2)$ ,  $C_s$ ; and  $\text{Fe}(\eta^1\text{-O}_2)$ ,  $C_{\infty v}$ . Molecular orbital and harmonic vibrational analyses were carried out for these species, in addition to Mulliken population analyses. Singly positive and negative charged species were also considered and fully geometry optimized in a self-consistent field (SCF) gradient method. Accurate ionization potentials and electron affinities (both vertical,  $v$ , and adiabatic,  $a$ , determinations) were thus able to be computed. The results show the following for the ground state (GS)  $\text{Fe}(\text{O})_2$ ,  $C_{2v}$ ,  $M = 3$ :  $\angle\text{OFeO} = 138.1^\circ$  ( $133.6^\circ$ ) [values in parentheses are for local spin density approximation (LSDA)–VWN, while the others are at the GGA-B88/P86 level]. Here,  $R_e \text{Fe-O} = 1.60 \text{ \AA}$  ( $1.57 \text{ \AA}$ ),  $\text{ET} = -1414.2064 \text{ au}$  ( $-1,410.5047 \text{ au}$ ),  $\text{EA}_a = 2.47$  ( $2.60$ ) eV,  $\text{IP}_a = 10.6$  ( $10.5$ ) eV,  $\text{EA}_v = 2.41$  ( $2.20$ ) eV,  $\text{IP}_v = 10.67$  ( $10.63$ ) eV, and  $\text{EA}_{\text{exp}} = 2.349$  eV (in agreement with related studies). In the GS the dioxygen molecule is found to be dissociated, compared to those states which have coordination modes where the  $\text{O}_2$  molecule formally persists. A  $3d4sp$  configuration for the iron atom is found to be especially relevant in Fe–O bond formation. The iron–oxygen and oxygen–oxygen bonds involved are characterized. A direct relationship is observed between these electronic and structural properties, influencing also the total energy for a given molecule. © 2000 John Wiley & Sons, Inc. Int J Quantum Chem 80: 307–319, 2000

**Key words:** metal–ligand interactions; DFT calculations; ionization potentials; electron affinities; Fe– $\text{O}_2$  systems

*Correspondence to:* M. Castro.  
Contract grant sponsor: DGAPA-UNAM.  
Contract grant number: PAPIIT IN-104798.

## Introduction

Molecular oxygen is involved in several reactions, both of biological and industrial importance, in which transition metals (TMs), especially iron, are essential. In these, TMs act as catalysts and are also involved in the activation, transport, and storage of molecular species as O<sub>2</sub> and H<sub>2</sub>. In particular, the understanding at a molecular level of such diverse processes as O<sub>2</sub> carrying in biological systems or corrosion of metals can be benefited from a deeper study of this type of metal–ligand interaction.

Theoretical studies exist on iron–oxygen systems, such as laser-ablated iron atoms in an oxygen/argon atmosphere [1], photooxidation reactions of pentacarbonyl iron [2], and models of more complex systems such as iron–porphyrin and other Fe–O moieties [3, 4].

Previous work [1, 2, 5–7] on iron–oxygen systems has revealed that the assignment of a ground state (GS) for FeO<sub>2</sub> is strongly dependent on the level of theory used. The results presented in Table I illustrate the discrepancies that arise between the descriptions of this small FeO<sub>2</sub> system as originated from different theoretical approaches.

As depicted in Table I, it is only until recent years that the Fe–O<sub>2</sub> systems have been studied ab initio by means of all-electron calculations performing both electronic and structural relaxations. Even at this high level of treatment the results show a dramatic dependence on the computational procedure employed.

Semiempirical calculations offer an incorrect geometry for the calculated GS. Moving to the treatments of the all-electron type, it is well known that the Hartree–Fock (HF) point of view alone is inadequate for an accurate description of systems

containing TMs. For instance, HF does predict a correct structure, C<sub>2v</sub>, for the FeO<sub>2</sub> GS [6]; however, the multiplicity observed ( $M = 7$ ) seems to be too high to allow the spin-pairing process or chemical bond formation. When correlation effects are taken into account, such as in [1, 2, 7], the description of the bonding in the GS molecule predicts more consistent results for the geometry. Nevertheless, there is some controversy on the electronic state of the GS of the FeO<sub>2</sub> system.

Despite the available ab initio studies including correlation effects [1, 2, 7], a systematic theoretical study is needed at a high level of theory which includes full structural and electronic optimization of the systems referred to and description of the bonds therein.

Open-shell transition metal systems present a challenge for the state-of-the-art computational methods and theories. In this regard, density functional theory (DFT), provided the use of suitable gradient-corrected functionals that accurately describe the exchange–correlation (XC) interactions, has given examples [8] of being one of the most reliable tools for their study. This is seen from both a computational procedure simplicity and a formal theory point of view. In a first step, transition-metal (TM-L) systems can be studied at the local spin density approximation (LSDA) of DFT [9]. However, the use of a generalized gradient approximation (GGA), such as that proposed by Becke for exchange [10] and Perdew for correlation [11], is more appropriate for that type of complex.

The present work deals with a systematic theoretical study on FeO<sub>2</sub>. Our treatment was done using DFT techniques (*vide infra*), and we believe that our research might help to elucidate some structural and electronic aspects of this molecule. The study involves the calculation of the structural parameters for the lowest energy states of several FeO<sub>2</sub> coordination modes. Furthermore, vibrational, molecular orbital, Mulliken population, and charge transfer analyses were carried out on these states in order to afford insight on the nature of the chemical bond in these species.

**TABLE I**  
Comparison between the different GSs for FeO<sub>2</sub> as reported in the literature.

Reference	Year	Ground state
MINDO [5]	1982	Fe(O) <sub>2</sub> , D <sub>∞h</sub> , M = 3
HF/STO-3G* [6]	1994	Fe(O) <sub>2</sub> , C <sub>2v</sub> , M = 7
DFT/STO [2]	1993	Fe(O) <sub>2</sub> , C <sub>2v</sub> or D <sub>∞h</sub> , M = 3
DFT-B3LYP [1]	1996	Fe(O) <sub>2</sub> , C <sub>2v</sub> , M = 3
MP2, CCSD(T)/TZV* [7]	1997	Fe(O) <sub>2</sub> , C <sub>2v</sub> , M = 1

## Methodology

First-principles, all-electron calculations were performed with the code DGauss 3.0.1 [12], which is a *linear combination of Gaussian-type orbitals* DFT-based method (LCGTO-DF). The DZVP2 orbital basis sets were used, namely (63321/5211\*/41+)

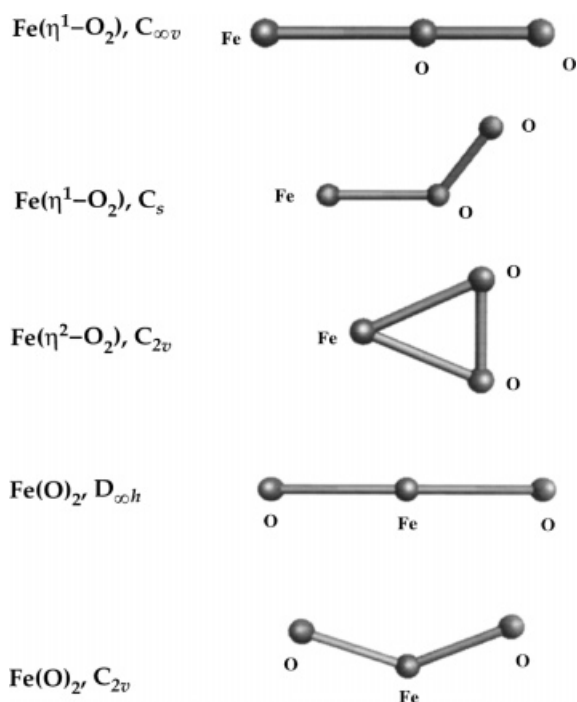


**FIGURE 1.** Coordination modes possible for the  $\text{FeO}_2$  system.

for Fe and (721/51/1) for O. Additionally, TZV-A1 (10/5/5) auxiliary basis sets were used for the fitting of the density and the XC contributions to the total energy and energy gradients.

The procedure involved full geometry optimization by a self-consistent field (SCF) energy gradient method of candidate structures (shown in Fig. 1) in different quantum states, first at the LSDA by using the Vosko–Wilk–Nusair (VWN, [9]) functional. The convergence criteria used were tight, i.e.,  $\Delta E = 1 \times 10^{-7}$  au for the total energy,  $\Delta\rho = 1 \times 10^{-5}$  au for the density, and  $\Delta E/\Delta r = 5 \times 10^{-5}$  au for geometry optimizations. A fine grid of 194 angular points per atom was employed for the numerical integration and second-derivative evaluation. Harmonic vibrational, molecular orbital, Mulliken population, and charge transfer analyses were then performed on the located lowest energy states for each coordination mode. In a second step, these structures were then fully reoptimized at the GGA level by use of the Becke (1988) exchange [10] and Perdew (1986) correlation [11] functionals. This XC scheme will be referred to as B88/P86. The same tight convergence criteria and fine numerical grid were used, and harmonic vibrational, molecular orbital, Mulliken population, and charge transfer analyses performed as in the former case. The same expen-

sive and thorough treatment was given to singly charged negative and positive states derived from the ground state.

Calculations were done with a Cray YMP4/464 supercomputer.

Five possible coordination modes for the dioxygen molecule with an iron atom were considered. These are shown in Figure 1. We have paid special attention to the location, in the potential energy surface of  $\text{Fe-O}_2$ , of that structure that shows a similar coordination mode and symmetry,  $\text{Fe}(\eta^1\text{-O}_2)$ ,  $C_s$ , as that found in oxyhemoglobin.

The UniChem package [13], coupled to DGauss, was used both for the launch of the calculations as well as for the visualization of the obtained results of geometries and molecular orbitals. This package is very useful to follow the structural and electronic changes during the geometry optimization procedure.

## Results and Discussion

The VWN and B88/P86 functionals yield the total energies for the states ordered in Table II, with values in hartrees.

Figure 2 shows the lowest energy state for each coordination mode considered at the LSDA level. Relative total energies between these states are also included, as well as structural parameters for each state.

Figure 3 shows the results for the lowest energy state for each coordination mode, as well as structural parameters and relative energies calculated at the GGA level. The differences in O–O distances from the coordinated  $\text{O}_2$  species and free  $\text{O}_2$  are shown in Figures 2 and 3.

The ordering of states is essentially the same for both levels of theory. The GGA produces slightly larger bond distances than LSDA. This is accounted for by the correction that the B88/P86 functional makes of the overestimation of bonding produced by the LSDA approach.

Another observation is that a pattern is found between total energy and both O–O and Fe–O bond distances. The lower the total energy for a given state, the larger the O–O distance and the shorter the Fe–O one. This implies a lowering of total energy for a state with increasing dissociation of the O–O bond and increasing formation of the Fe–O bond.

The bond orders calculated, presented in Table III, show a similar picture as that observed in the structural parameters. The limit case is that of

**TABLE II**  
**Total energies in hartrees for the FeO<sub>2</sub> series of compounds and their labeling.**

State	LSDA-VWN	GGA-B88/P86
Vc, Fe( $\eta^1$ -O <sub>2</sub> ), C <sub>∞v</sub> , M = 5	see IIIb	
Vb, Fe( $\eta^1$ -O <sub>2</sub> ), C <sub>∞v</sub> , M = 3	see IVa	
Va, Fe( $\eta^1$ -O <sub>2</sub> ), C <sub>∞v</sub> , M = 7	-1410.3679916	
IVd, Fe( $\eta^1$ -O <sub>2</sub> ), C <sub>s</sub> , M = 1	see IIIc	
IVc, Fe( $\eta^1$ -O <sub>2</sub> ), C <sub>s</sub> , M = 5	see IIIb	
IVb, Fe( $\eta^1$ -O <sub>2</sub> ), C <sub>s</sub> , M = 7	see IIIc	
IVa, Fe( $\eta^1$ -O <sub>2</sub> ), C <sub>s</sub> , M = 3	-1410.3887	-1414.1010 <sup>a</sup>
IIIc, Fe( $\eta^2$ -O <sub>2</sub> ), C <sub>2v</sub> , M = 1	—	-1414.1004
IIIb, Fe( $\eta^2$ -O <sub>2</sub> ), C <sub>2v</sub> , M = 7	-1410.3879	-1414.1207
IIIa, Fe( $\eta^2$ -O <sub>2</sub> ), C <sub>2v</sub> , M = 5	-1410.4091	-1414.1118
IIIa, Fe( $\eta^2$ -O <sub>2</sub> ), C <sub>2v</sub> , M = 3	-1410.4213	-1414.1207
Id, Fe(O) <sub>2</sub> , C <sub>2v</sub> , M = 7	-1410.4216	-1414.1332
IId, Fe(O) <sub>2</sub> , D <sub>∞h</sub> , M = 5	see IB	-1414.1473
Ic, Fe(O) <sub>2</sub> , C <sub>2v</sub> , M = 1	-1410.4866	-1414.1796
Ib, Fe(O) <sub>2</sub> , C <sub>2v</sub> , M = 5	-1410.4948	-1414.1955
Ia, Fe(O) <sub>2</sub> , D <sub>∞h</sub> , M = 3	-1410.4970 <sup>b</sup>	-1414.2006 <sup>b</sup>
Ia, Fe(O) <sub>2</sub> , C <sub>2v</sub> , M = 3	-1410.5047	-1414.2064

<sup>a</sup> Medium convergence criteria; for the tight convergence criteria result see IIIa.

<sup>b</sup> Two negative vibrational frequencies.

the lowest total energy structure or the GS, which presents the strongest Fe–O bond order of 0.99 (1.06) at the GGA (LSDA) level of theory and the weakest O–O bond order of the set of states.

In the GS, Ia, there is effectively no O–O bond left, with respect to free O<sub>2</sub>. In contrast, state IIIa presents a lesser activation of O<sub>2</sub> as the difference between bond orders of the free species and the coordinated one is of a unit (there is still molecularity of dioxygen present in state IIIa). Another proof of evidence is provided by the charge transfer in these species (see Table IV) as there exists a direct relationship between increasing Fe → O charge transfer and lower total energy, at both levels of theory used, with the limit case being the GS, Ia, with a net charge transfer of 0.831 (0.756) of a unit.

Table V shows the progressive increase in 4p participation to the global Fe configuration in a given state with decreasing total energy for that state.

The results obtained from the harmonic vibrational analyses performed on the black species in Table II are shown in Table VI.

### GROUND STATE, Ia

Our computed GS for Fe(O)<sub>2</sub> has a triangular structure of C<sub>2v</sub> symmetry and M = 3. In this state, the binding between the O atoms is negligible,

while the bond order analysis indicates the appearance of a single bond between Fe and each O. These bonds have equilibrium bond lengths of 1.60 Å, and the O–Fe–O angle formed is of 138.1° at the GGA level of theory. This picture is in agreement with the results obtained by Andrews et al., who used the B3LYP hybrid functional [1]. They also obtain a C<sub>2v</sub> structure, with M = 3, for the GS of FeO<sub>2</sub>. Their results for the Fe–O bond lengths and O–Fe–O angle are very similar to our computed values.

Table VII compares structural parameters for several proposed GSs of Fe(O)<sub>2</sub> in a C<sub>2v</sub> symmetry, as reported in the literature and those obtained through the present study.

Our DFT results are in disagreement with those obtained by means of Hartree–Fock calculations where the correlation effects were included through configuration interaction (CI) techniques [7]. The CI treatment indicates that the GS of Fe–O<sub>2</sub> is a closed-shell state, M = 1, in C<sub>2v</sub> symmetry, with Fe–O bond lengths of 1.50 Å and an O–Fe–O angle of 169.8°. That is, the CI GS of Fe–O<sub>2</sub> is closer to a linear structure than the DFT one. Looking at the bond lengths and bond angles, the CI results overestimate, with respect to DFT, the bonding in the O–Fe–O molecule. Indeed, the CI M = 1 state implies a major chemical bond formation (pairing of electrons) than

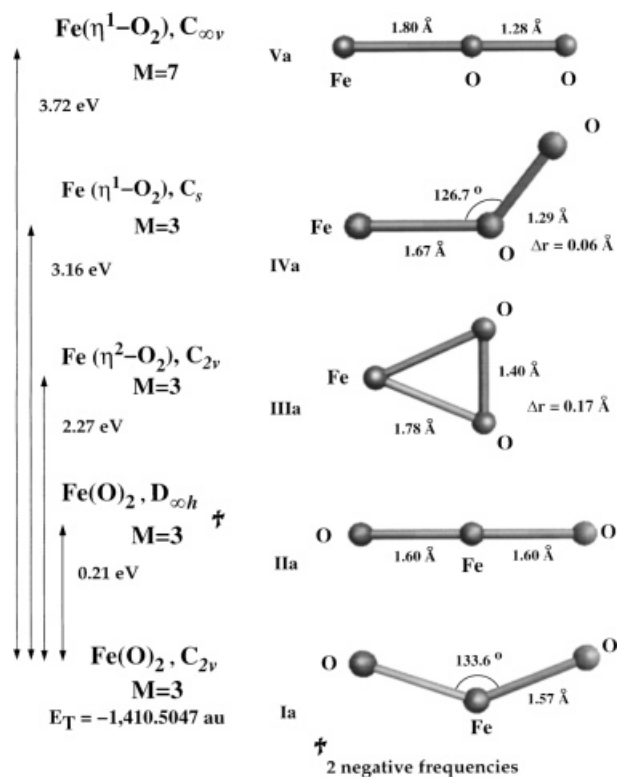


**FIGURE 2.** Structural parameters and relative energies calculated by geometry optimizations for the lowest energy states for  $\text{Fe}(\text{O})_2$ ,  $C_{2v}$ ;  $\text{Fe}(\text{O})_2$ ,  $D_h$ ;  $\text{Fe}(\eta^2\text{-O}_2)$ ,  $C_{2v}$ ;  $\text{Fe}(\eta^1\text{-O}_2)$ ,  $C_s$ ; and  $\text{Fe}(\eta^1\text{-O}_2)$ ,  $C_v$ , at the LSDA-VWN level of theory.

the DFT  $M = 3$  state. However, our calculations reveal that the singlet state is located 0.73 eV above our computed  $M = 3$  GS.

It is interesting to observe that the quintet state is located only +0.30 eV above the GS, at the B88/P86

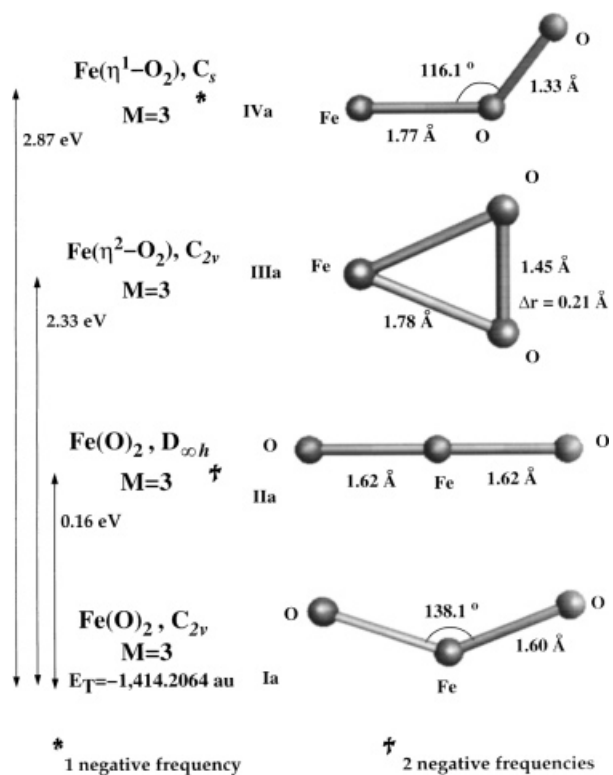


**FIGURE 3.** Structural parameters and relative energies for results of geometry optimizations of compounds of the  $\text{FeO}_2$  system at the GGA-B88/P86 level of theory.

level of theory. A similar picture was obtained by Andrews et al. Their results indicate that the triplet and quintet states are almost degenerate, since the quintet is located only 0.1 eV above the triplet, using the Becke-Perdew functional [1]. However, the use of the hybrid B3LYP functional gives a reverse order: the quintet is the GS, with the triplet lying

**TABLE III**  
Mayer bond orders calculated for the  $\text{FeO}_2$  series of compounds.

State	Functional	Fe-O	O-O
$\text{O}_2$	VWN		1.4743
$M = 3$	B88/P86		1.4675
Va, $\text{Fe}(\eta^1\text{-O}_2)$ , $C_{\infty v}$ , $M = 7$	VWN	0.5829	0.9420
IVa, $\text{Fe}(\eta^1\text{-O}_2)$ , $C_s$ , $M = 3$	VWN	0.5939	0.4444
IIIa, $\text{Fe}(\eta^2\text{-O}_2)$ , $C_{2v}$ , $M = 3$	VWN	0.6390	0.4767
	B88/P86	0.5847	0.4632
IIa, $\text{Fe}(\text{O})_2$ , $D_{\infty h}$ , $M = 3$	VWN	0.7162	-0.5117
	B88/P86	0.8943	0.2257
Ia, $\text{Fe}(\text{O})_2$ , $C_{2v}$ , $M = 3$	VWN	1.0523	0.1926
	B88/P86	0.9930	0.1933

**TABLE IV**  
Charge transfer in the FeO<sub>2</sub> set of states.

State	Functional	Fe	O1	O2
Va, Fe( $\eta^1$ -O <sub>2</sub> ), C <sub>∞v</sub> , M = 7	VWN	0.374	-0.250	-0.124
IVa, Fe( $\eta^1$ -O <sub>2</sub> ), C <sub>s</sub> , M = 3	VWN	0.337	-0.162	-0.176
IIIa, Fe( $\eta^2$ -O <sub>2</sub> ), C <sub>2v</sub> , M = 3	VWN	0.536	-0.268	-0.268
	B88/P86	0.611	-0.305	-0.305
IIa, Fe(O) <sub>2</sub> , D <sub>∞h</sub> , M = 3	VWN <sup>a</sup>	0.818	-0.409	-0.409
	B88/P86 <sup>a</sup>	0.877	-0.439	-0.439
Ia, Fe(O) <sub>2</sub> , C <sub>2v</sub> , M = 3	VWN	0.756	-0.378	-0.378
	B88/P86	0.831	-0.416	-0.416

<sup>a</sup> Two negative vibration frequencies.

+0.1 eV above the quintet [1]. As pointed out by Andrews et al., the quintet state is not compatible with the experiment, since the calculated O–Fe–O angle (of 142°) obtained for the triplet is more consistent with the experiment than the O–Fe–O angle for the quintuplet (118°). Hence, the Becke–Perdew picture of Andrews et al., and ours indicate that the GS of O–Fe–O is more likely to be a triplet state.

These studies reveal that the results obtained on systems that contain TM atoms are very sensitive to the level of theory used for XC effects. A similar conclusion has been reached before [14] in our studies of small TM clusters. In this particular O–Fe–O case, it seems that the Becke–Perdew scheme works much better than the B3LYP one. This is a surprising result, since the B3LYP functional has proven to yield results of chemical accuracy in benchmark calculations, even though these calculations involve systems that do not contain TM atoms [15, 16]. This means that more accurate functionals need to be developed for a better description of TM systems and, consequently, of the XC effects which arise in them.

**TABLE V**  
Iron configurations for different states as obtained through Mulliken population analysis.

Label	Functional	Iron configuration
Va	VWN	[Ar]4s <sup>1.02</sup> 4p <sup>0.293</sup> 3d <sup>6.31</sup>
IVa	VWN	[Ar]4s <sup>0.777</sup> 4p <sup>0.155</sup> 3d <sup>6.731</sup>
	B88/P86	[Ar]4s <sup>0.74</sup> 4p <sup>0.171</sup> 3d <sup>6.819</sup>
IIIa	VWN	[Ar]4s <sup>0.472</sup> 4p <sup>0.135</sup> 3d <sup>6.819</sup>
	B88/P86	[Ar]4s <sup>0.503</sup> 4p <sup>0.142</sup> 3d <sup>6.819</sup>
IIa	VWN	[Ar]4s <sup>0.514</sup> 4p <sup>0.43</sup> 3d <sup>6.329</sup>
	B88/P86	[Ar]4s <sup>0.512</sup> 4p <sup>0.279</sup> 3d <sup>6.278</sup>

There are experimental observations [1] that suggest a triplet GS for Fe(O)<sub>2</sub>, instead of a singlet or a quintet. As mentioned above, Andrews et al. found that the O–Fe–O angle for the GS had a defined range of values in which only the triplet species fit. Furthermore, the observed isotopic 16/18 frequency ratios [1], for the antisymmetric and symmetric modes of the triplet state, show excellent agreement with theoretical values using both Becke–Perdew and B3LYP schemes. On the other hand, their calculated values for the quintet for both functionals were termed incompatible with the experimental ratios. Despite this, the authors point out that since both states are close in energy, more experimental studies are needed to corroborate or deny that the triplet is the true GS. In comparison, the mentioned MP2/CCSD(T) [7] results show a poor match with the experimental picture quoted above.

Of all the Fe(O)<sub>2</sub> sets of candidates, the found GS, Ia, has the strongest Fe–O bond and the weakest (negligible) O–O bond. This state also shows the greatest Fe → O charge transfer, which accounts for its high stability or lowest energy. Moreover, the Mulliken population analysis reveals that the electronic pattern of the Fe atom is of 3d4s4p type. In particular, the GS has the most important 4p participation.

In effect, state Ia, Fe(O)<sub>2</sub>, C<sub>2v</sub>, M = 3, has considerably lost the molecularity of O<sub>2</sub>. This can be seen in the frontier molecular orbitals (MOs) depicted in Figure 4 as well as in the vibrational modes illustrated in Figure 5 which correspond to an angular inserted dioxide species.

As is observed in comparison to other states, a pattern is established between lower total energy for a given state and its increasing Fe–O bond formation and Fe → O charge transfer. This lowering

**TABLE VI**  
Harmonic vibrational frequencies and intensities for the lowest energy states of each coordination mode in the  $\text{FeO}_2$  series.<sup>a</sup>

State	Theory level	Frequency ( $\text{cm}^{-1}$ )	Intensity ( $\text{km/mol}$ )
$\text{O}_2$	LSDA	1590.57	0.0
$M = 3$	GGA	1520.1	0.0
Va, $\text{Fe}(\eta^1\text{-O}_2)$ , $C_{\infty v}$ , $M = 7$	LSDA	1337.46	138.05
		434.96	5.37
		162.88	2.4
IVa, $\text{Fe}(\eta^1\text{-O}_2)$ , $C_s$ , $M = 3$	LSDA	1267.28	279.61
		607.26	7.13
		159.42	3.25
	GGA	-22.8	2.41
		565.8	3.87
		113.4	288.6
IIIa, $\text{Fe}(\eta^2\text{-O}_2)$ , $C_{2v}$ , $M = 3$	LSDA	1026.82	61.83
		767.64	10.03
		527.13	34.11
	GGA	915.46	52.93
		615.75	13.43
		479.43	0.33
IIa, $\text{Fe}(\text{O})_2$ , $D_{\infty h}$ , $M = 3$	LSDA	1078.27	217.43
		920.54	0.00
		-196.93	28.95
		-196.93	28.95
	GGA	1024.28	182.42
		874.87	0.00
		-165.6	29.86
		-165.6	29.86
Ia, $\text{Fe}(\text{O})_2$ , $C_{2v}$ , $M = 3$	LSDA	1087.1	178.65
		970.74	29.2
		225.8	17.2
	GGA	1043.6	23.7
		918.4	23.7
		201.2	20.7

<sup>a</sup> Tight convergence criteria as well as a fine numerical integration grid, were employed.

**TABLE VII**  
Comparison of the structural parameters calculated for the GS Ia and those reported in the literature.

$\text{Fe}(\text{O})_2$ , $C_{2v}$	$R_e$ , Fe-O ( $\text{\AA}$ )	$\angle\text{OFeO}$
HF/STO-3G* [6], $M = 7$	1.93	40.0
DFT/B3LYP [1], $M = 3$	1.58	141.5
MP2, CCSD(T)-TZV* [7], $M = 1$	1.52	162.3
B88/P86, $M = 3$ , Ia	1.60	138.1

of total energy is coupled to a decrease of the O–O bonding and to a greater  $4p$  and  $4s$  participation in the characteristic overall  $3d4sp$  configuration for the iron atom in a given state.

Mulliken population analysis on the valence MOs for the GS shows that the principal contributions to the bonds are of a  $3d4sp(\text{Fe})-2p(\text{O})$  nature. For instance, the highest occupied MO (HOMO) is of a bonding nature and contains 27% of its electronic density on the  $4s$  orbital of Fe, 15% on orbital  $3d_{y^2}$ , 7.6% on orbital  $3d_{x^2}$ , 5% on orbital  $3d_{z^2}$ , 5%

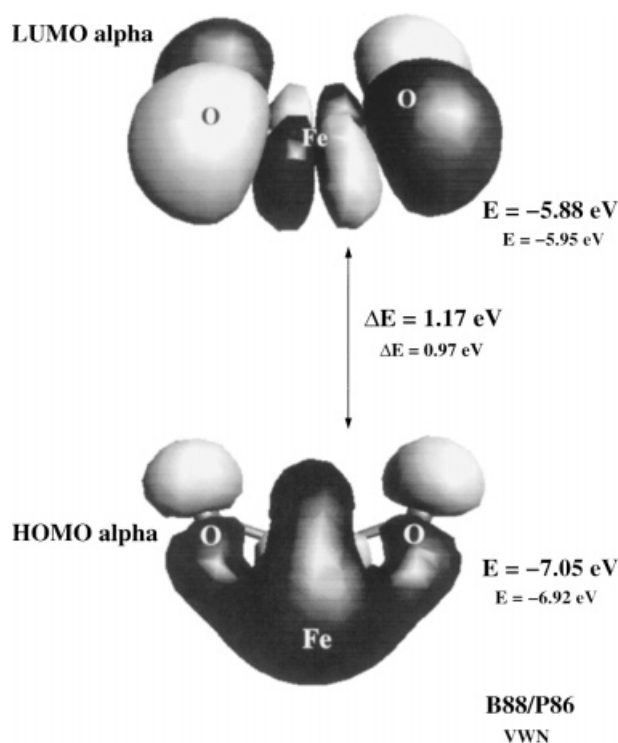


**FIGURE 4.** Frontier MOs for the GS, Ia. The  $3d4sp$  configuration on the iron atom is seen in the HOMO orbital.

on orbital  $3p_y$ , and 1.8% on orbital  $3d_{xy}$  of the same atom. The resting 40% of the electronic charge is shared evenly between each oxygen in orbitals  $2p_x$  and  $2p_y$ . On the other hand, the lowest unoccupied MO (LUMO) is antibonding and is composed of 43.3% of electronic density on orbital  $3d_{xz}$  of iron and 28% on orbital  $2p_z$  of each oxygen. The  $3d4sp$  (of Fe) and  $2p$  (of O) contributions to the bonding are noticeable in the drawings of the HOMO and LUMO, displayed in Figure 4.

The population analysis reveals that the GS has a magnetic moment located mainly on the Fe atom. This moment corresponds to the two  $3d$  electrons that were not involved in the bond-forming process.

The vibrational pattern for the GS of  $\text{FeO}_2$  is characteristic of a  $C_{2v}$  structure and is illustrated in Figure 5.

In a similar fashion to Table VII, Table VIII compares vibrational frequencies for several  $\text{Fe}(\text{O})_2$ ,  $C_{2v}$  GSs. The present work yields harmonic vibrational analysis results in the same order of magnitude and compare well to those of Andrews et al. [1] calculated using the B3LYP functional and those observed experimentally [1] and with calculations of MP2, CCSD(T)-TZV quality [7] cited in Table VIII.

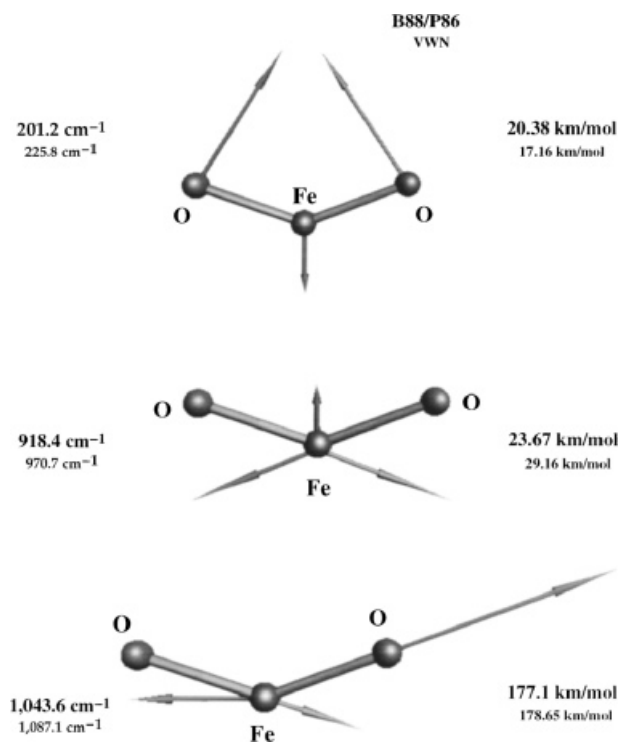


**FIGURE 5.** Harmonic vibration modes, frequencies, and intensities for the GS, Ia, at the LSDA-VWN and GGA-B88/P86 levels of theory.

The frequencies were assigned to the bands produced by  $\text{FeO}_2$  species present in the laser ablation of iron atoms in an oxygen atmosphere. The assignment fits with a  $C_{2v}$  structure where there is no longer a significant O–O bond.

A series of singly, positive and negative, charged states (derived from the GS) were also searched, both with and without structural relaxation, that is, through full SCF geometry optimizations and single-point SCF calculations, respectively. This made possible the determination of precise and accurate ionization potentials (IPs) and electron affini-

**TABLE VIII**  
Comparison between the harmonic vibrational frequencies for the GS Ia and those reported in the literature.

$\text{Fe}(\text{O})_2$ , $C_{2v}$	Vibrational frequency ( $\text{cm}^{-1}$ )
DFT/B3LYP [1], $M = 3$	958.3, 891.3, 194.3
MP2, CCSD(T)-TZV* [7], $M = 1$	1182.8, 1176.7, 173.5
B88/P86, $M = 3$ , Ia	1043.6, 918.4, 201.2

**TABLE IX**  
Properties calculated for the GS and a comparison with an experimental value.

	LSDA-VWN	GGA-B88/P86	Experimental [1]
Vertical determinations			
Ionization potential ( $\text{IP}_v$ )	10.63	10.67	
Electron affinity ( $\text{EA}_v$ )	2.20	2.41	2.358
Horizontal determinations			
Ionization potential ( $\text{IP}_h$ )	10.50	10.57	
Electron affinity ( $\text{EA}_h$ )	2.60	2.47	

ties (EAs), which may be connected with the corresponding experimental determinations of these properties.

Vertical (single-point calculations, allowing no structural relaxation of the system) and horizontal (adiabatic, involving geometry optimization, i.e., structural relaxation of the system) determinations of IPs and EAs are presented in Table IX, which has values in electron-volts.

There is a very small change in structural parameters from the neutral species to the charged ones (in the horizontal determinations). The GSs for both the negative ( $\text{FeO}_2^-$ ) and positive ( $\text{FeO}_2^+$ ) species had the same geometry (inserted angular dioxide) and symmetry ( $C_{2v}$ ) as the neutral GSs. Both negative and positive GSs resulted in doublets,  $M = 2$ , one resulting from the addition and the other from the subtraction, respectively, of an electron from the neutral,  $M = 3$ , GS.

If we compare the calculated vertical EA at the GGA level of 2.410 eV with the experimental value [1] of 2.358 eV, we find a small difference of 2.2%. This result encourages the use of a B88/P86 scheme for the study of physical and physicochemical properties of systems that require an accurate description, such as those in which TMs are present.

### STATE IIa

As mentioned, we have also located some higher energy states of the neutral  $\text{FeO}_2$  molecule. In what follows we will briefly discuss these findings in systems which can be of relevance in processes in which they are encountered.

State IIa has structural parameters and energy values very close to those present in the GS. Nevertheless, this linear dioxo species has peculiarities such as two degenerate negative vibrational frequencies at both levels of theory used. This indicates that such a species is not at a true minimum of en-

ergy, even though it lies close in energy (0.16 eV at the B88/P86 level) to the GS.

This result confirms state Ia as the true GS and extends the knowledge of this system from that obtained in other studies such as [2], where similar structures as Ia and IIa were proposed as possible GSs.

### STATE IIIa

This triangular species contains the molecular dioxygen unit, which is reflected in its calculated HOMO and LUMO orbitals (Fig. 6) and its vibrational modes (Fig. 7).

In IIIa, the perturbation of the O–O bond, though strong, is not enough for dissociative activation as occurs in the GS. The IIIa state lies considerably higher in energy, 2.33 eV (at the B88/P86 level of theory) above the GS. Such high location is consistent with the longer Fe–O bond length and smaller Fe–O bond order as compared to those found in the GS.

Although both the HOMO and LUMO (shown in Fig. 6) are antibonding, they both show fragments of molecular  $\text{O}_2$  units;  $\pi_g^*$  in the former and  $\pi_g$  in the latter. The HOMO is composed of 30.3% of the electronic density on the  $d_{xy}$  iron orbital, in addition to 34.8% of this density on each oxygen  $p_y$  orbital. In contrast, the LUMO has 64.5% of density on the 4s orbital, 27.8% on orbital  $4p_z$ , and 5.6% on orbital  $d_{z^2}$ . Each oxygen atom takes 2.6% of the total electron density of the LUMO orbital on orbitals  $2p_z$ . Overall, these MOs show how the  $3d4sp$  contributions of the Fe atom are involved in the bonding with the  $\pi$  component of the oxygen atoms.

Besides having a higher total energy than the GS, the species IIIa has less charge transfer (which resides in back donation from iron  $d$  orbitals to oxygen molecular orbitals) and less  $4p$  participation in the iron configuration than in state Ia.

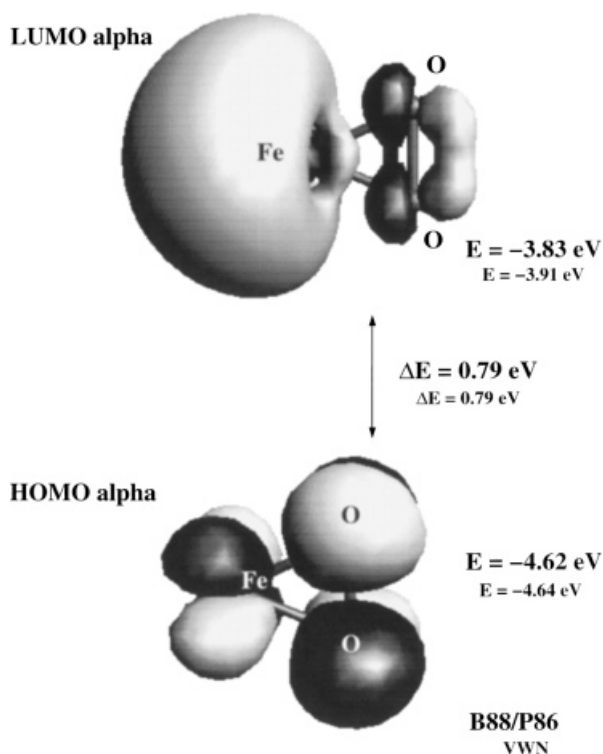


**FIGURE 6.** Frontier MOs for the species  $\text{Fe}(\eta^2\text{-O}_2)$ ,  $C_{2v}$ ,  $M = 3$ , IIIa. Note the MO between oxygen atoms in both HOMO and LUMO figures, revealing a  $\pi_g^*$  fragment in the former case and a  $\pi_u$  in the latter. The  $3d4sp$  configuration of iron is seen in the LUMO orbital.

The values framed in Figure 7 represent the mode which is possible to identify with the dioxygen molecule vibration. The frequency displacement from the value in the free  $\text{O}_2$  molecule is presented, displaying an activation for this subunit in the molecule where the dioxygen molecule is trapped by an iron atom. This activation is evidenced in the lower frequency, larger O–O bond distance, and smaller bond order for the O–O bond in IIIa than in the free  $\text{O}_2$  molecule.

The observed frequencies [1] of this  $\text{Fe}(\text{O})_2$ ,  $C_{2v}$ , state may be assigned to our calculated values. The strongest observed band for this state,  $956 \text{ cm}^{-1}$ , and a weaker band,  $548.4 \text{ cm}^{-1}$ , are reasonably close to our estimations,  $915.5$  and  $615.8 \text{ cm}^{-1}$ , respectively. This agreement suggests that the triplet state is the one of lowest energy for this  $\text{Fe}(\text{O})_2$  coordination mode. A similar assignment was done by Andrews et al. [1], but instead of a triplet, they found that the quintet state, although it is a high energy state, fits better than the triplet. Indeed, in the calculations of Andrews et al., the septet is the lowest energy state, followed by the quintet and triplet states. As

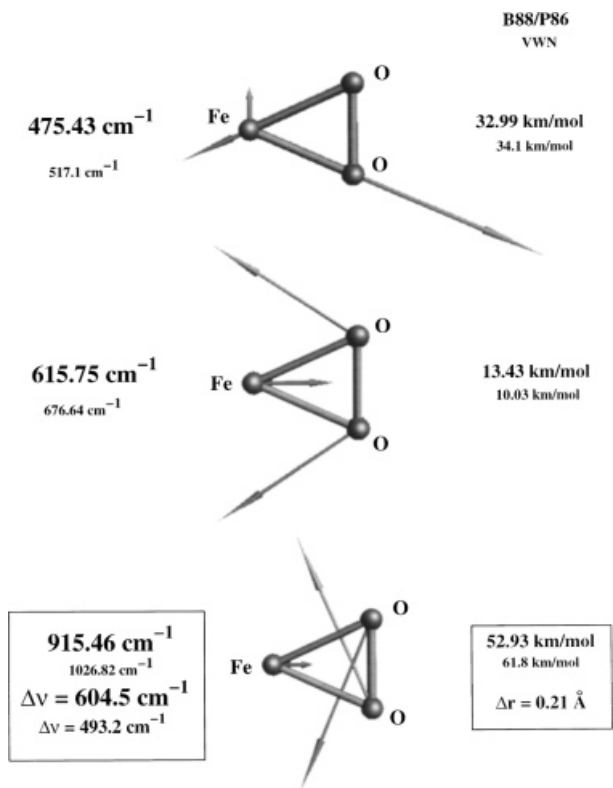


**FIGURE 7.** Harmonic vibrational analysis results for the species  $\text{Fe}(\eta^2\text{-O}_2)$ ,  $C_{2v}$ ,  $M = 3$ , IIIa, at the LSDA-VWN and GGA-B88/P86 levels of theory.

pointed out by the authors [1], the B3LYP scheme is biased toward high spin states. This picture exemplifies that the descriptions of TM-L systems depend sensitively on the chosen functional. Our results show the consistency of the B88/P86 XC scheme as implemented in the DGauss program, both in the determination of the lowest energy states and in the vibrational assignments.

The so-called energy of dissociation is the difference in energy between the lowest energy state containing the bound molecular  $\text{O}_2$  species and the GS where this molecularity no longer exists. For the present work, this difference occurs from state IIIa to state Ia and amounts to  $2.27 \text{ eV}$  ( $52.35 \text{ kcal/mol}$ ) at the LSDA-VWN level, or  $2.33 \text{ eV}$  ( $53.79 \text{ kcal/mol}$ ) at the GGA-B88/P86, which are roughly half of that reported in the MINDO study [5]. This result suggests that the dissociation of a molecule of  $\text{O}_2$  by a single iron atom is a less unlikely process as predicted by the MINDO study [5]. Experimentally, it has been shown that for this process to happen, a sufficiently excited iron atom has to be present to successfully react with a dioxygen molecule.

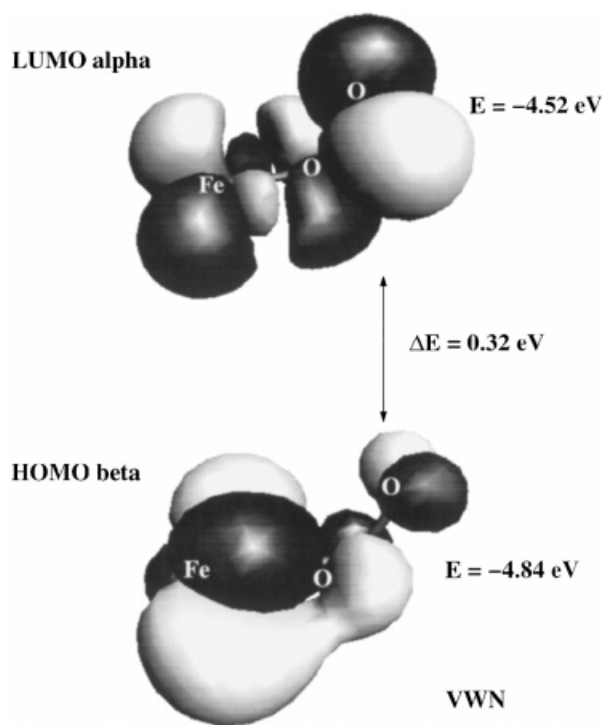


**FIGURE 8.** Frontier MOs for the species  $\text{Fe}(\eta^1\text{-O}_2)$ ,  $C_s$ ,  $M = 3$ , IVa. Note that the region between oxygen atoms in the HOMO orbital contains  $\text{O}_2$  antibonding MO fragment, even though in total the HOMO is actually of a bonding nature between Fe and O subunits. This particular MO shows the way in which charge transfer of the type  $d\pi_g^*$  can occur.

### STATE IVa

The coordination mode and symmetry of the state IVa are very similar to those that occur in oxyhemoglobin, in which the chemical environment of the protein's active centers is provided by the heme groups, which are embedded and bonded to its globin structures.

A single-point B88/P86 calculation (with tight energy and density convergence criteria) reveals that IVa has a negative vibrational frequency at  $-22.8 \text{ cm}^{-1}$ , while the positive frequencies are 565.8 and  $1113.4 \text{ cm}^{-1}$ . This result differs from that of Andrews et al. [1], who found that IVa is a true minimum since it has three positive frequencies: 134.7, 472.7, and  $1159.8 \text{ cm}^{-1}$ . Using a lower level of theory, as in the LSDA approach, we have also found that IVa has three positive frequencies: 159.4, 607.3, and  $1267.3 \text{ cm}^{-1}$ . Note that in this last case the smallest value is very close to that of Andrews et al. Then, our higher level of theory calculation indicates that IVa is a transition state (TS).

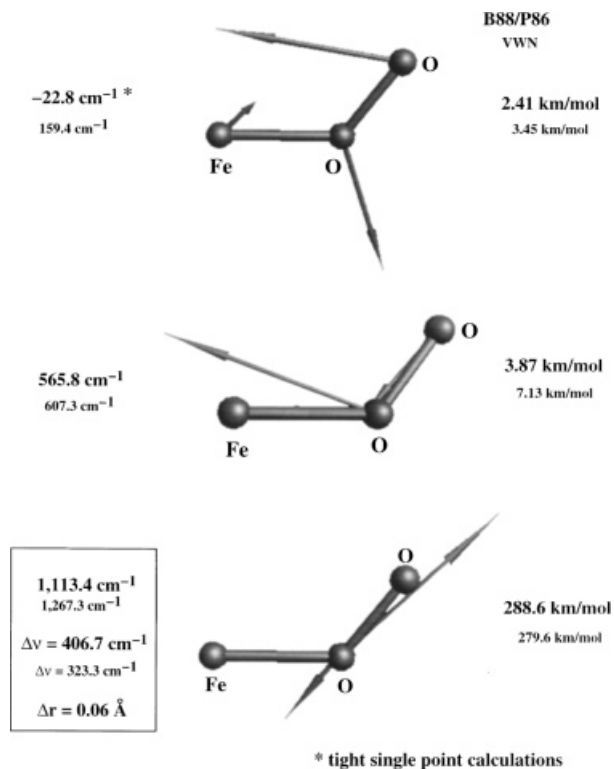


**FIGURE 9.** Results from the harmonic vibrational analysis on the species  $\text{Fe}(\eta^1\text{-O}_2)$ ,  $C_s$ ,  $M = 3$ , IVa.

The TS nature of IVa is reflected by the fact that a geometry optimization (at the GGA level with a tight convergence criterion) led to a structure with coordination mode and symmetry  $\text{Fe}(\eta^2\text{-O}_2)$ ,  $C_{2v}$  (by closure of the  $\text{FeOO}$  angle), which eventually fell to the lower energy IIIa state.

The HOMO for IVa is bonding, while the LUMO is antibonding. In HOMO (see Fig. 8) the  $\text{O}_2$  molecular fragment interacts through its  $\pi$  antibonding orbitals with the  $3d$  orbitals of the Fe atom. In this bonding interaction a considerable  $d \rightarrow \pi_g^*$  charge transfer is recognized.

The vibrational analyses for IVa produce the results depicted in Figure 9. The mode which is highlighted presents the activation of the O–O bond, which is of less extent than that present in state IIIa. The vibrational mode possessing a negative frequency can also be seen in Figure 9. As shown above, the present work predicts an angular inserted dioxide species as the GS for the  $\text{Fe}(\text{O})_2$  system, 2.87 eV (at the B88/P86 level) lower than state IVa. Specific conditions in the hemoglobin environment render a special stability to the IVa moiety.

### STATE Va

This linear high-multiplicity molecule owes its total spin number of 6 to the absence of pairing between the two free electrons on O<sub>2</sub> and four free electrons on iron. This mode of coordination, therefore, does not have important interactions between dioxygen and iron and, consequently, lies high in energy with respect to states corresponding to other modes.

---

### Conclusions

A correct ordering by total energy of the different states and coordination modes of the FeO<sub>2</sub> series was constructed.

The Fe(O)<sub>2</sub>, C<sub>2v</sub>, M = 3, GS Ia predicted by the present work is in agreement with experimental and theoretical evidence, as is another work previously published elsewhere [1]. Our analysis of Fe(O)<sub>2</sub> illustrates that a proper treatment of the XC effects is critical to the accurate description of the structural and electronic properties of transition metal systems such as Fe–O<sub>2</sub>.

There is a clear pattern found between lower energy for a given state and the increased formation of Fe–O bonds, increased activation of the oxygen–oxygen bond, increased charge transfer of an Fe → O type, and electronic configurations 3d4sp with increasing participation of 4s and 4p electronic charge on iron.

Charge transfer in the form of back donation from iron *d* orbitals to oxygen  $\pi$  antibonding molecular orbitals generates the diminishing of the O–O bond.

The participation of 4p orbitals in the iron configuration provides polarization for the metal atom, which allows it to form strong bonds with each oxygen atom. Participation of 4s orbitals affords delocalization of electronic charge, which in turn also favors the Fe–O bonding.

The calculated GS Ia can be seen as the last stage in a process of nearing the O<sub>2</sub> molecule to an iron atom. This O<sub>2</sub>-to-Fe approach may be seen to lead to lowering the total energy for the system. While the O<sub>2</sub> molecule transversally approaches the iron atom, lowering the total energy for a given state due to the formation of Fe–O bonds, there is a progressive breaking of the O–O bond coupled to a buildup of the Fe–O bonding. This process eventually carries to the dissociative adsorption of the dioxygen molecule by a sufficiently excited Fe atom, which is the

case of the most stable moiety, the GS. Indeed, the electronic pattern of the Fe atom, in the GS of FeO<sub>2</sub>, is of 3d<sup>7</sup>4s<sup>1</sup>4p<sup>x</sup> nature, which differs from the 3d<sup>6</sup>4s<sup>2</sup> configuration of the free Fe atom.

Triangular structures such as IIIa lie higher in energy than the angular inserted dioxo species such as Ia.

An Fe( $\eta^1$ -O<sub>2</sub>), C<sub>s</sub> moiety can be present in systems such as oxyhemoglobin, probably due to the steric and electronic factors affecting the central iron atom which prevent the formation of iron–dioxo bonds (such as those present in the GS Ia) which are lower in energy than angular Fe–(O<sub>2</sub>) structures of the type of IVa. Besides securing stabilization of the  $\eta^1$ -O<sub>2</sub>, C<sub>s</sub> moiety, these steric and electronic factors might be responsible for the reversibility of the Fe–O union, compulsory for the dioxygen transport process, as this  $\eta^1$ -O<sub>2</sub>, C<sub>s</sub> moiety is in an irregular well of potential energy.

The value of 2.2% in error between the calculated figure and the experimental one for electron affinity validates this study and affords it as a useful method to study other systems of the same kind with more metallic atoms and other substrate molecules such as H<sub>2</sub>, N<sub>2</sub>, NH<sub>3</sub>, NO, etc.

### ACKNOWLEDGMENTS

Financial support from DGAPA-UNAM under project PAPIIT IN-104798 and supercomputing resources from DGSCA (UNAM) are greatly acknowledged. One of us (A.T.G.-S.) would like to thank Programa 127 "Formación Básica en la Investigación" for a scholarship.

---

### References

1. Andrews, L.; Chertihin, G. V.; Ricca, A.; Bauschlicher, C. W., Jr. *J Am Chem Soc* 1996, 118, 467–470.
2. Lyne, P. D.; Mingos, D. M.; Ziegler, T.; Downs, A. J. *Inorg Chem* 1993, 32, 4785–4796.
3. Shu, L. J.; Nesheim, J. C.; Kauffman, K.; Munck, E.; Lipscomb, J. D.; Que, L. *Science* 1997, 275, 515–518.
4. Rovira, C.; Ballone, P.; Parrinello, M. *Chem Phys Lett* 1997, 271, 247–250.
5. Blyholder, G.; Head, J.; Ruetter, F. *Inorg Chem* 1982, 21, 1539–1545.
6. Helmer, J. M. C.; Plane, J. *J Chem Soc Faraday Trans* 1994, 90, 395.
7. Solà, M.; Duran, M.; Cao, Z. *Chem Phys Lett* 1997, 274, 411–421.
8. Salahub, D. R.; Castro, M.; Fournier, R.; Mlynarski, P.; Papai, I.; St-Amant, A.; Ushio, J. In *Density Functional Methods*

- in Chemistry; Labanowski, J. K.; Andzelm, J. W., Eds.; Springer: New York, 1991.
- Vosko, S. H.; Wilk, L.; Nusair, M. *Can J Phys* 1980, 58, 1200.
  - Becke, A. D. *Phys Rev A* 1988, 38, 3098.
  - Perdew, J. P. *Phys Rev* 1986, 8822; *Phys Rev B* 1991, 7406E.
  - Andzelm, J. W. In *Density Functional Methods in Chemistry*; Labanowski, J. K.; Andzelm, J. W., Eds.; Springer: New York, 1991.
  - Dixon, D. A.; Fitzgerald, G.; Raeuchle, T. In *Data Visualization in Molecular Science*; Addison-Wesley: New York, 1995. UniChem is a commercial package available from Oxford Molecular.
  - Jamorski, C.; Martinez, A.; Castro, M.; Salahub, D. R. *Phys Rev B* 1997, 55, 10905.
  - Lee, C.; Yang, W.; Parr, R. G. *Phys Rev B* 1988, 37, 785.
  - Miehlich, B.; Savin, A.; Stoll, H.; Preuss, H. *Chem Phys Lett* 1989, 157, 200.